European Journal of Pharmaceutical Sciences 192 (2024) 106650

Contents lists available at ScienceDirect

European Journal of Pharmaceutical Sciences

journal homepage: www.elsevier.com/locate/ejps

The use of polymorphic state modifiers in solid lipid microparticles: The role of structural modifications on drug release performance

Serena Bertoni [a], Elena Simone [b], Stefano Sangiorgi [a], Beatrice Albertini [a,*], Nadia Passerini [a]

[a] Department of Pharmacy and Biotechnology, University of Bologna, Via S. Donato 19/2, Bologna 40127, Italy
[b] Department of Applied Science and Technology, Politecnico di Torino, Torino 10129, Italy

ARTICLE INFO

Keywords:
Spray congealing
Tristearin
Microspheres
Polymorphism
Solid-state
Synchrotron SAXS
Controlled release

ABSTRACT

This study investigates the correlation between the structural and release properties of solid lipid microparticles (MPs) of tristearin containing 5 % w/w of four different liquid additives used as crystal modifiers: isopropyl myristate (IM), ethyl oleate (EO), oleic acid (OA) and medium chain triglycerides (MCT). All additives accelerated the conversion of the unstable α-form of tristearin, formed after the MPs manufacturing, to the stable β-polymorph and the transformation was completed within 24 h (for IM and EO) or 48 h (for OA and MCT). The kinetic of polymorphic transition at 25 °C was investigated by simultaneous synchrotron SAXS/WAXS and DSC analysis after melting and subsequent cooling of the lipid mixture. After crystallization in the α-phase, additives accelerate the solid-solid phase transformation to β-tristearin. SAXS data showed that two types of structural modifications occurred on MPs during storage: compaction of the crystal packing (slight decrease in lamellar thickness) and crystal growth (increased number of stacked lipid lamellae). The release behavior of a model hydrophilic drug (caffeine) at two different amounts (15 % and 30 %) from MPs was studied in water and biorelevant media simulated the gastric and intestinal environment. It was particularly significant that the introduction of IM, EO and MCT were able to prolong the drug release in water, passing from a diffusion-based Higuchi kinetics to a perfect zero-order kinetic. Moreover, the overall release profiles were higher in biorelevant media, where erosion/digestion of MPs was observed. After 6 months, a moderate but statistically significant change in release profile was observed for the MPs with IM and EO, which can be correlated with the time-dependent structural alterations (i.e. larger average crystallite size) of these formulations; while MPs with OA or MCT displayed stable release profiles. These findings help to understand the correlation between release behavior, polymorphism and supramolecular-level structural modification of lipid formulations containing crystal modifiers.

1. Introduction

Solid lipids are more and more commonly used as modified drug delivery excipients in the pharmaceutical industry. Solid lipid sustained-release systems include tablets (Abdelbary and Tadros, 2008), pellets (Thomsen et al., 1993), microspheres (Bertoni et al., 2020; Jaspart et al., 2007), hot-melt coated systems (Barthelemy et al., 1999) and implants (Vollrath et al., 2017), which are capable of controlling the release of hydrophilic drugs. However, the poor long-term stability of such formulations represents a critical issue from the industrial point of view. Most solid lipid excipients, in which triacylglycerols (TAGs) play a crucial role as major components, exist at the solid state in three main crystalline forms, namely α, β' and β, in order of stability (Fig. 1). As this polymorphism is of monotropic type, the crystallization into unstable forms during melting-based processes implicates that there will be a transition towards more stable forms overtime. The rearrangement of the lipid during long-term storage determines multiple changes that might affect the drug release properties of the dosage form.

A recent strategy to overcome this issue exploits specific additives that work as crystal modifiers of the lipid, i.e. substances able to induce the conversion of the lipid into the most stable crystalline form, thereby avoiding further polymorphic transitions. Different oral-approved liquid lipids (LL) added at 10 % to tristearin-based microparticles promoted the transition from the α to the stable β form with a kinetic varying from few minutes to days, depending on the specific LL (Bertoni et al., 2021). The introduction of 10 to 30 % of Polysorbate 65 to a lipid coating based

* Corresponding author.
E-mail address: beatrice.albertini@unibo.it (B. Albertini).

https://doi.org/10.1016/j.ejps.2023.106650
Received 30 June 2023; Received in revised form 18 October 2023; Accepted 20 November 2023
Available online 22 November 2023

on tripalmitin have shown to cause polymorphic transformation into the stable β-form after the hot melt coating process, even using low process temperatures (25–35 °C) (Becker et al., 2016; Lopes et al., 2017). In both cases, the use of polymorphic state modifiers allowed to obtain polymorphically stable lipid formulations without the application of high process temperatures or post-process thermal treatments (e.g. annealing).

Nevertheless, the introduction of such additives to the lipid matrix might influence various attributes of the dosage form, first of all the drug release. The introduction of 10 % LL led to higher release rates as compared to analogue formulations containing only pure tristearin (Bertoni et al., 2021). The same tendency was observed for tripalmitin-polysorbate 65 mixture-based lipid coated particles, where the release of N-acetylcysteine increased significantly passing from 10 % to 30 % of polysorbate 65 (Lopes et al., 2017). In order to extend the release of this formulation, the thickness of the coating layer was increased from 50 % to 70 % (Lopes et al., 2017). This modification allowed a more gradual release; however, the release profiles were unstable upon storage despite tripalmitin was already in the β-polymorph (Lopes et al., 2017). Thus, prolonging the release of the drug by higher coating thickness seems to correspond to a more relevant release alteration upon storage. This trend was noted also in a recent study about hydroclorothiazide coated with the same tripalmitin-polysorbate 65 mixture at three coating levels (15, 25, and 60 %) (Schertel et al., 2021a). The alteration in drug release after storage, as indicated by the similarity factors, increased substantially with the coating amount in the formulation.

Two aspects emerged from these findings. First, instability problems are more relevant for lipid-based systems formulated to extend the release of drugs, rather than to provide immediate release. A sustained-release system, in fact, should gradually release a reproducible amount of drug over an extended period of time, and when this process relies on a solid lipid used as retard material, even small alterations of the lipid structure would produce important fluctuations in the release performance. Secondly, it is becoming increasingly clear that drug release can be unstable despite the stable molecular packing of the lipid. Thus, in addition to polymorphic transitions, there must be other factors responsible for the instability of lipid-formulations during storage. Recent studies have identified structural alterations at supra-molecular levels as possible sources of instability. Drug release instability of tripalmitin-based lipid coating was explained by considering the crystal growth followed by phase separation of components of the formulation during storage (Lopes et al., 2017). Similarly, Paudel and co-workers observed that the increase in drug release from spray congealed-microspheres of Compritol 888 ATO was related with growth in the pore size as well as with phase separation of Poloxamer, used as pore former, from the main lipid (Kushwah et al., 2022, 2020). These alterations affect in turns the bulk properties of the dosage form, such as surface area, density and porosity (Lopes et al., 2015). Drug release instability has also been related to modifications in the surface morphology (i.e. lipid blooming) observed on storage (Khan and Craig, 2004). Blooming of TAGs upon storage are reported to create water-repellent surfaces characterized by higher contact angle. As for example, the contact angle of water droplets on tristearin surface is 150° for the bloomed β-form with respect to 110° for the α-form (Fang et al., 2007). A recent study from Pluntze et al. (2023) highlights the concurrent roles of surface properties (mostly wettability) and pore network properties (including porosity, tortuosity, pore connectivity, etc) in dictating the drug release profiles from tristearin microparticles in various polymorphic forms.

Therefore, despite the potential advantages of using polymorphic state modifiers to stabilize lipid-based formulations, there are still important hurdles that limit their applications. The main difficulty lies in obtaining a sufficiently sustained release pattern of the hydrophilic drugs as well as a good control of the numerous structural modifications of the lipid during storage.

This study investigates the structural and release properties of solid lipid microparticles (MPs) of tristearin containing liquid additives acting as polymorphic state modifiers. MPs were produced by spray congealing technology either with pure tristearin (SSS, Fig. 1) or with SSS enriched by 5 % w/w of liquid lipids. Four different liquid lipids, isopropyl myristate, ethyl oleate, oleic acid and medium chain triglycerides (Fig. 1), were selected based on a previous study, where they showed to promote SSS conversion in the stable β-form immediately after the process if used at 10 % w/w (Bertoni et al., 2021), but also greatly increased the drug release. As the final product attributes and performance depend on how the lipid organizes at various structural hierarchical levels, MPs properties were investigated by different techniques (DSC, PXRD, synchrotron SAXS/WAXS) focusing on the influence of each crystal modifier on the lipid structural properties and their evolution during storage. Then, the release properties of MPs loaded with caffeine as model hydrophilic drug at two amounts (15 and 30 % w/w)

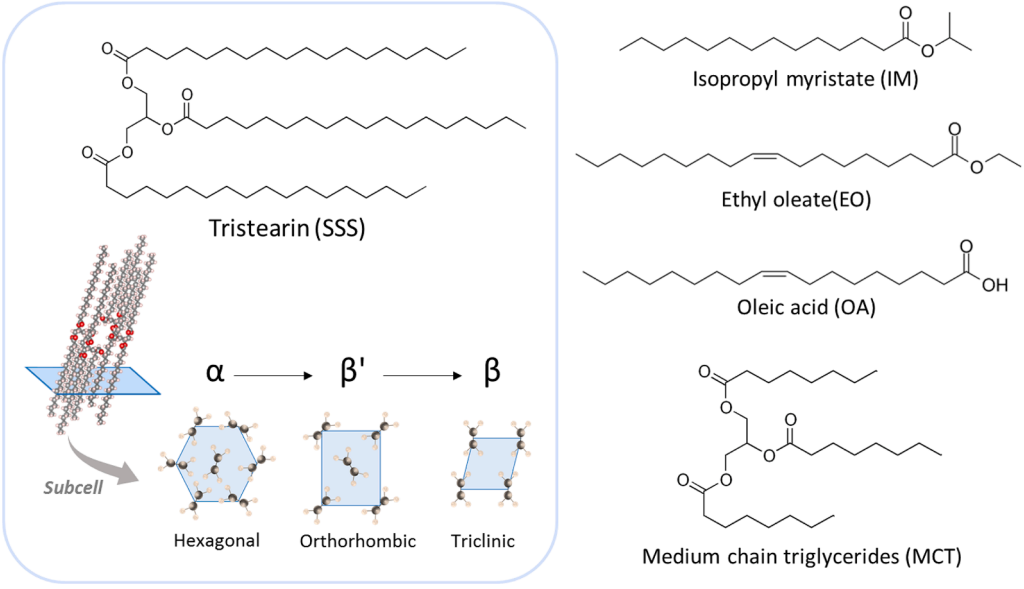

Fig. 1. Molecular structure of tristearin and subcell structure models of its three polymorphic forms. Molecular structures of isopropyl myristate, ethyl oleate, oleic acid and medium chain tryglicerides.

were studied. In the totality of the previous studies, only water, aqueous solutions or phosphate buffers were used as dissolution media, which are not representative of the biological fluids upon oral route administration. Therefore, in order to provide insights into the impact of physiological conditions on the release performances of lipid MPs, drug release tests were performed, beside water, in biorelevant media containing lipases to resemble the gastric and intestinal fasted conditions. Finally, alterations in drug release profiles after storage were evaluated and correlated with modifications of the lipid crystalline structure.

2. Materials and methods

2.1. Materials

Tristearin (SSS, Dynasan®118, purity 99 %) was kindly provided by IOI Oleo (Witten, Germany). For β-SSS, Dynasan®118 was used as received. α-SSS was obtained by melting tristearin at 90 °C followed by rapid cooling to room temperature. Caffeine (CAF) was purchased from Sigma-Aldrich (Steinheim, Germany). Isopropyl myristate (IM) were obtained from Fluka (Buchs, Switzerland). Ethyl oleate (EO) and oleic acid (OA) were purchased from Carlo Erba Reagents (Milan, Italy). Medium chain trigycerides (MCT, Labrafac™ lipophile WL 1349) was supplied from Gattefossè (Milan, Italy). Taurocholic acid sodium salt hydrate (99 % TLC, 3.9 % water, MW = 537.68 g/mol anhydrous base) was kindly supplied by Prodotti Chimici Alimentari (Basaluzzo, Italy). Pepsin from porcine gastric mucosa (tested according to Ph.Eur), L-α-Phosphatidylcholine from egg yolk (Lecithin, 76.1 % TLC), pancreatin from porcine pancreas (8 × USP specifications) were purchased from Sigma Aldrich (Steinheim, Germany).

2.2. MPs production by spray congealing

MPs were prepared by spray congealing, using the wide pneumatic nozzle (WPN) as atomization device. Briefly, SSS was melted at the temperature 10 °C above its melting point and the additive was added to obtain a one-phase lipid melt. The liquid mixture was subsequently transferred into a temperature-controlled feeding tank placed above the spray-congealing nozzle pre-heated to 10 °C above the melting temperature of SSS. The atomization of the lipid mixture was then obtained at 1.5 bar air pressure and nozzle temperature of 85 °C. The atomized molten droplets solidified into a cooling chamber at room temperature. Batch dimension was 10 g. The process yield (%) was calculated based on the amount of MPs collected after the process with respect to the batch size. The MPs were stored in sealed 15 ml polyethylene bottles at room temperature and protected from light (25 °C, 60 % RH). For CAF-loaded MPs, crystalline CAF powder was added to the molten lipid mixture in order to obtain MPs with a theoretical drug loading of 15 or 30 % w/w. Then, the suspension was stirred and atomized to form MPs using the same process parameters.

2.3. Differential scanning calorimetry (DSC)

DSC analysis was performed with a Perkin-Elmer DSC 6 (Perkin Elmer, Beaconsfield, UK). Before measurements, the instrument was calibrated with indium and lead for the temperature, and with indium for the enthalpy. Non-hermetic aluminum pans and lids (Perkin Elmer, Beaconsfield, UK) with an operating range of −170° to 600 °C and a volume of 40 μL were used. Six to ten milligrams of sample was accurately weighted and placed into the aluminum pan, then the lid was applied without hermetic sealing and without pinhole. The analysis was performed under a nitrogen flow of 20 mL/min. In order to check for the polymorphic form of MPs, a simple heating scan was performed. As the α-form and the β-form of SSS have melting temperature in the range 50–55 °C and 70–74 °C, respectively, the heating ramps were performed from 25 °C to 90 °C using a scanning rate of 10 °C/min.

2.4. Powder X-ray diffraction (PXRD)

Samples were analysed by X-ray powder diffraction technique using a Philips X'Pert powder diffractometer equipped with a graphite monochromator in the diffracted beam. CuKα radiation was used (40 mA, 40 kV) and the spectra were obtained in the range 3–30° of 2θ.

2.5. Scanning Electron Microscopy (SEM)

The shape and surface morphology of MPs before and after release studies were assessed by means of SEM. Samples were fixed on the sample holder with double-sided adhesive tape. SEM images were obtained using a Zeiss Scanning Electron Microscope Model EVO 50 EP. The samples were observed without coating in EP mode with a chamber pressure of 90 Pa and an acceleration voltage of 10 kV.

2.6. Synchrotron small and wide angle light scattering

Small and Wide Angle X-ray Scattering (SAXS/WAXS) analysis were performed at the Austrian SAXS beamline of the ELETTRA Synchrotron (Trieste, Italy). Measurements were performed using a Pilatus3 1M detector for the SAXS signal, and a Pilatus 100k detector for the WAXS-range.

Two different experimental setups were utilized:

a) A SAXS/WAXS coupled with simultaneous DSC measurement setup was used to monitor the kinetic of polymorphic transitions of MPs *in situ*. The incident beam energy was set at 8 keV (SAXS range from a q-value of 0.08 to ca. 6 nm^{-1}, WAXS range from a q-value of 10 to ca. 16.5 nm^{-1}. Images were collected continuously with a time resolution of 60 s (20 s of exposition time). MPs were loaded into quartz capillaries of 1.5 mm outer diameter (Hilgenberg, Maisfeld, Germany) and inserted into an in-line micro-calorimeter having a small window to allow the synchrotron radiation to pass the sample capillary (Kalnin et al., 2005; Ollivon et al., 2006). MPs samples were subjected the sample to a 4-steps thermal profile consisting in: heating ramp from 25 to 90 °C at 10 °C/min; isothermal step at 90 °C for 5 min; cooling ramp from 90 to 25 °C at 10 °C/min and isothermal step at 25 °C for 120 min.
b) Systematic static SAXS measurements were performed at 25 °C on MPs after 1 week after production (referred as time 0, t_0), and after 6 months of storage at 25 °C/60 % RH (t_6). MPs samples were loaded into glass capillaries of 1.5 mm outer diameter (Hilgenberg, Maisfeld, Germany). These measurements were performed at SAXS range from a q-value of 0.08 to ca. 6 nm^{-1}.

2.7. SAXS data processing

Data analysis was carried out with OriginPro2022 (OriginLab, Massachusetts). The Bragg peaks (first, second and third order) corresponding to the different SSS lamellar structure were identified in the SAXS patterns. Each peak was individually processed by applying a baseline correction and then fitted using Voigt function. The peaks maxima (q values) were plotted against their corresponding Miller index and linearly interpolated. The characteristics lamellar d-spacing (in nm) was obtained using the slope of the fitted line q in the formula:

$$d = \frac{2\pi}{q} \tag{1}$$

The average size (D) of the SSS crystallites was estimated based on the first-order SAXS peak using the Scherrer equation, which relates the diffraction peak broadening to the size of sub-micrometer crystallites (Acevedo et al., 2012; Lopes et al., 2015):

$$D = \frac{K\lambda}{FWHM(2\theta)\ cos\theta} \tag{2}$$

where, FWHM (full width at half maximum) is the width in radians of the diffraction maximum measured at half-height between the background and the peak, θ is the diffraction angle and λ is the wavelength of the X-rays. K (Scherrer constant) is a dimensionless number determined by the crystallite shape; in the absence of detailed shape information, $K = 0.9$ is a good approximation. The values of FWHM were calculated by fitting the raw data by a Voigt function.

The number of stacked SSS lamellae in each sample can be calculated by dividing the average crystallite size (D) by the d-spacing (d) (Schertel et al., 2021a, 2021b).

2.8. Determination of drug content

The amount of encapsulated CAF was determined on MPs with defined size (diameters in the range 250–355 μm). Specifically, for each formulation, MPs with size of 250–355 μm were separated by sieve analysis from the rest of the batch using two sieves with the desired mesh size (Scientific Instrument, Milan, Italy) and a vibrating shaker (Octagon Digital, Endecotts, London, UK).

Briefly, 15 mg of MPs were accurately weighed and added to 20 mL of purified water. The suspension was heated to melt the carrier and then shaken for 1 h. Finally, the solution was filtered, diluted with the same solvent and the drug content was assayed spectrophotometrically at 273 nm using a Cary-60 UV-vis spectrophotometer (Agilent Technologies GmbH, Waldbronn, Germany). A calibration curve was prepared with CAF concentrations of 1–100 μg/mL ($R^2 = 0.9996$). At least three samples were analyzed for each formulation and results were reported as mean ± s.d.

2.9. In vitro drug release test

In vitro drug release studies were performed under sink condition using compendial method with USP II paddle dissolution apparatus (DT 800 Erweka GmbH, Heusenstamm, Germany). To eliminate the contribution of the MPs surface area on release profiles, only MPs with a narrow range of diameters (250–355 μm) were used. For the release test, 40 mg or 80 mg of MPs containing 30% or 15% CAF, respectively, were transferred into the dissolution vessel containing 500 mL of dissolution medium in order to have a total CAF concentration of 25 μg/mL. Dissolution media used were purified water, Fasted State Simulated Gastric Fluid (FaSSGF) and Fasted State Simulated Intestinal Fluid (FaSSIF). FaSSGF at pH 1.6 containing pepsin (0.1 mg/mL) and FaSSIF containing pancreatin (6.0 mg/mL, equal to 100 U/mL considering lipase activity) at pH 6.5 were prepared according to Klein (Klein, 2010) as summarized in Table S1. The selected pancreatin concentration is suggested by United States Pharmacopoeia 2009 in simulated intestinal fluid (Borde et al., 2012). Release studies were performed using the paddle rotation speed of 100 rpm. 2 mL of samples were withdrawn at 15, 30, 45, 60, 90, 120, 150, 180, 210, 240, 270 and 300 min using an 8 μm filter to avoid the removal of the MPs. CAF concentration in the collected samples was measured by UV–vis spectroscopy (λ_{max} of 273 nm) in case of water and FaSSGF, while CAF quantification in FaSSIF was performed by HPLC, using a method already reported (Albertini et al., 2019). The HPLC system consisted of two mobile phase delivery pumps (LC-10ADvp, Shimadzu, Japan), a UV–vis detector (SPD-10Avp, Shimadzu, Japan) and an autosampler (SIL-20 A, Shimadzu, Japan). A reversed phase C12 column (Synergi MAX-RP, 4 μm, 150 mm x 4.60 mm; Phenomenex, Bologna, Italy) was used as stationary phase, while the mobile phase consisted in 87.5 % sodium acetate buffer (50 mM, pH 4.0) and 12.5 % acetonitrile with a flow rate of 1 ml/min. The injected volume was 20 μl and the detection wavelength was set at 273 nm.

Thereafter, the experimental drug release profiles were fitted into a range of kinetic models: zero-order, first-order, Higuchi and Hixson–Crowell models. For each model, both the release rate constants (k) and correlation coefficients (R^2) were determined by using each of the models' equations, reported in Table S2.

2.10. Stability of MPs

Samples of MPs were stored for 6 months under long-term condition (25 °C/60 % R.H., t_6). The release profiles after storage were performed using water as dissolution medium and compared with the initial release profile using the similarity factor (f_2), according to the equation:

$$f2 = 50 * log\left\{1 + \left[\frac{1}{n} * \sum_{t=1}^{n} (R_t - T_t)^2\right]^{-0.5} * 100\right\} \quad (3)$$

where, n is the sampling number, R_t and T_t are the cumulative percentage dissolved of the reference and the test products at each time point t. Two dissolution profiles are considered similar if the f_2 value is between 50 and 100.

3. Results and discussion

3.1. Modification of the kinetics of polymorphic transition of MPs caused by additives

MPs of SSS alone or with 5 % w/w of additives were successfully produced by spray congealing with process yield between 65 and 77 % (Table S3), reasonable values in relation to the size (10 g) of the MPs. DSC analysis were performed on MPs with additives immediately after the process and at fixed time points (after 1, 3, 6, 24, 48 h) to evaluate the polymorphic evolution of freshly-prepared MPs. Fig. 2A showed that the thermal profiles of MPs analysed right after production presented a weak endothermic peak at 50–55 °C related to the melting of the α-form, followed by an exothermic event attributed to β crystallization upon heating. Both events indicate the presence of a certain residual amount of metastable α-SSS crystals in the sample. Finally, β-SSS (either formed during the scan or already present in the sample) melted at about 73 °C. MPs with 5 % additive showed a conversion into the stable β polymorph in timescales ranging 24–48 h (Fig. 2A). The two fatty esters (EO and IM) determined the highest rate of polymorphic transition. The complete conversion of MPs with 5 % additives after 48 h from production was further confirmed by PXRD (Fig. 2B), whereas pure SSS MPs were still in the α-form.

The kinetic of polymorphic transition was investigated by synchrotron SAXS/WAXS/DSC analysis. MPs that showed the fastest polymorphic conversion in the off-line DSC measurements (SSS_IM) were compared with MPs without additive (SSS) and the results are shown in Fig. 3. The combination of thermal analysis and X-ray scattering allowed to follow simultaneously the evolution of the lamellar structure in the SAXS region, the type unit cell in the WAXS region and the thermal behavior of the sample by DSC signal. Moreover, the experimental setup can detect time-resolved SAXS/WAXS spectra and DSC signal with extremely high signal-to-noise ratio and precision, while subjecting the sample to the desired thermal profile, represented in Fig. 3A. MPs were melted at 90 °C and then rapidly cooled (−10 °C/min) to 25 °C. SSS crystallized during the cooling step, as evident by the appearance of the first-order SAXS peak at about 47–48 °C, followed by the appearance of the second and third-order SAXS peaks, as evident in Fig. S1. The crystallization event was also evident as sharp exothermic peak in the DSC measurement in Fig. 3B. Both samples crystallized in a single lamellar phase with similar, but not identical, *d-spacing* (50.5 Å and 50.2 Å for SSS and SSS_IM, respectively), corresponding to the α-SSS phase (α-SSS reference sample presents a lamellar thickness of 50.3 Å, see Figs. 4 and S2A). The hexagonal α-phase was evident also in the WAXS region by the reflection at $q = 15.17$ nm^{-1} ($d = 4.14$ Å), reflecting the intramolecular distance between aliphatic chains. Whereas the cooling phase was similar between the two samples (Fig. S1A and B), interesting differences were observed in the SAXS/WAXS spectra during the

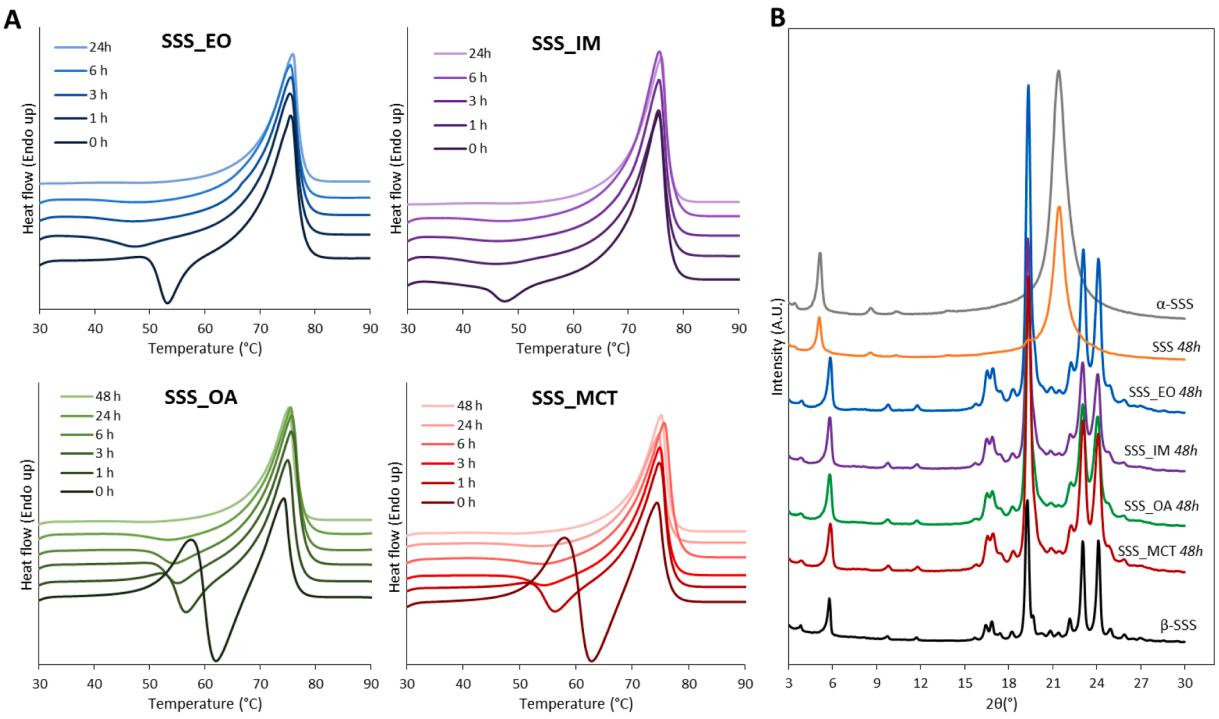

Fig. 2. (A) Polymorphic evolution of freshly prepared MPs containing 5 % w/w additives (SSS_EO, SSS_IM, SSS_OA and SSS_MCT) monitored by DSC analysis. (B) PXRD patterns of MPs without and with 5 % w/w additives after 48 h from production compared to α-SSS and β-SSS.

isothermal phase at 25 °C for MPs with (Fig. 3C) and without (Fig. 3D) additive. MPs of only SSS remained in the α-form for 2 h at 25 °C (Fig. 3D). Instead, the polymorphic transition caused by 5 % IM started at about 5 min minutes after reaching the final temperature of 25 °C, as shown from the appearance of a second lamellar phase with *d-spacing* of 45.3 Å (grey arrows). This new phase corresponds to β-SSS, as it presents an almost identical lamellar thickness to β-SSS reference sample, equal to 44.8 Å (Figs. 4 and S2A). The α→β polymorphic transformation was further confirmed by the WAXS data. Increasing reflections with the typical short-spacings of β-SSS were observed at 4.61 Å, 3.86 Å, and 3.70 Å (white arrows), while the α reflection at 4.14 Å concurrently decreased. It can be noted that this transformation caused a weak exothermic signal in the DSC measurement (zoomed in area on Fig. 3B).

Overall, crystal modifiers caused a rapid solid-solid polymorphic transformation towards the stable polymorph. Specifically, using a cooling rate of −10 °C/min followed by an isothermal phase at 25 °C, the transformation started at ambient temperature and involved the direct conversion of α-SSS to β-SSS, without any intermediate crystal structure (e.g., the β'-form).

3.2. Structural alterations of MPs during long-time storage

Synchrotron-SAXS analysis was performed on the MPs after 7 days after production, when the polymorphic transformation was complete (t_0) and after 6 months of storage at 25 °C and 60 % RH (t_6). The analysis allowed to detect changes in the structural organization of SSS in MPs in the length-scale 10–80 nm, i.e. the lamellar structure, as well as to estimate the average number of stacked SSS lamellae in each crystallite, i.e. the crystallite size.

3.2.1. Lamellar organization

The Bragg peaks (first, second and third order) found in the SAXS patterns evidenced the lamellar structure of SSS crystals (Fig. 4). Lamellae are formed by the longitudinal stacking of SSS molecules and correspond to a double- or triple- chain lengths (2 L or 3 L). By plotting the peak maximum positions as a function of their Bragg reflection order, a straight line with slope equal to the value of the *d-spacing* was obtained (Fig. S2). For SSS, SAXS spectra indicated a 2 L structure with a lamellar thickness of 50.3 Å for the α-form and 44.8 Å for the β-crystal, which is denser due to the tilting of SSS molecules, as schematized in Fig. 4. In the β-form of SSS the hydrocarbon chains are tilted at an angle of approximately 60° with respect to the planes formed by the end methyl groups (Merker and Daubert, 1964; Van Langevelde et al., 2001).

The SAXS pattern of MPs without additives showed, at t_0, one lamellar phase corresponding to α-SSS (*d-spacings* of 51.0 Å). Only a minor curvature of the SAXS curve was detected (black arrow, Fig. S3A), which might indicate the beginning of the α→β conversion. After storage, SSS was still mostly in the α-form, confirming that the slow conversion of pure SSS to the β-form. SAXS reflections with lower intensity, corresponding to a second lamellar phase, can be observed at t_6. After peak deconvolution analysis (Fig. S3B), the calculated *d-spacings* of this lamellar phase was 46.3 Å, whereas that of the α lamellar phase decreased from 51.0 to 50.6 Å. PXRD data confirmed that this second lamellar phase was β-SSS and gradually grew during storage (Fig. S4).

As expected, MPs with crystal modifiers showed only one crystalline phase corresponding to β-SSS at t_0. The calculated *d-spacings* were only slightly higher than that of reference β-SSS (Table 1), with differences within 1 Å. Nevertheless, it can be observed that the lamellar thickness increased in the order MCT>OA≈EO>IM, that is the same rank-order observed for the α→β conversion rate (Fig. 1A), suggesting that the effect of the additives in speeding up the conversion caused a slight variation in the lamellar organization of β-SSS. After long-time storage of MPs, the *d-spacing* values decreased of about 0.1 Å for all samples. This might indicate a gradual compaction of the crystal structure through a better packing of SSS molecules, possibly due to a phase separation of the liquid additives from β-SSS.

3.2.2. Crystallite size and growth

Multiple SSS lamellae stack on top of one another to form crystallites, or nanoplatelets (Acevedo and Marangoni, 2015). The thicknesses of these nanoplatelets can be calculated by considering the broadening of the first order SAXS peak, using Scherrer's equation, which is suitable

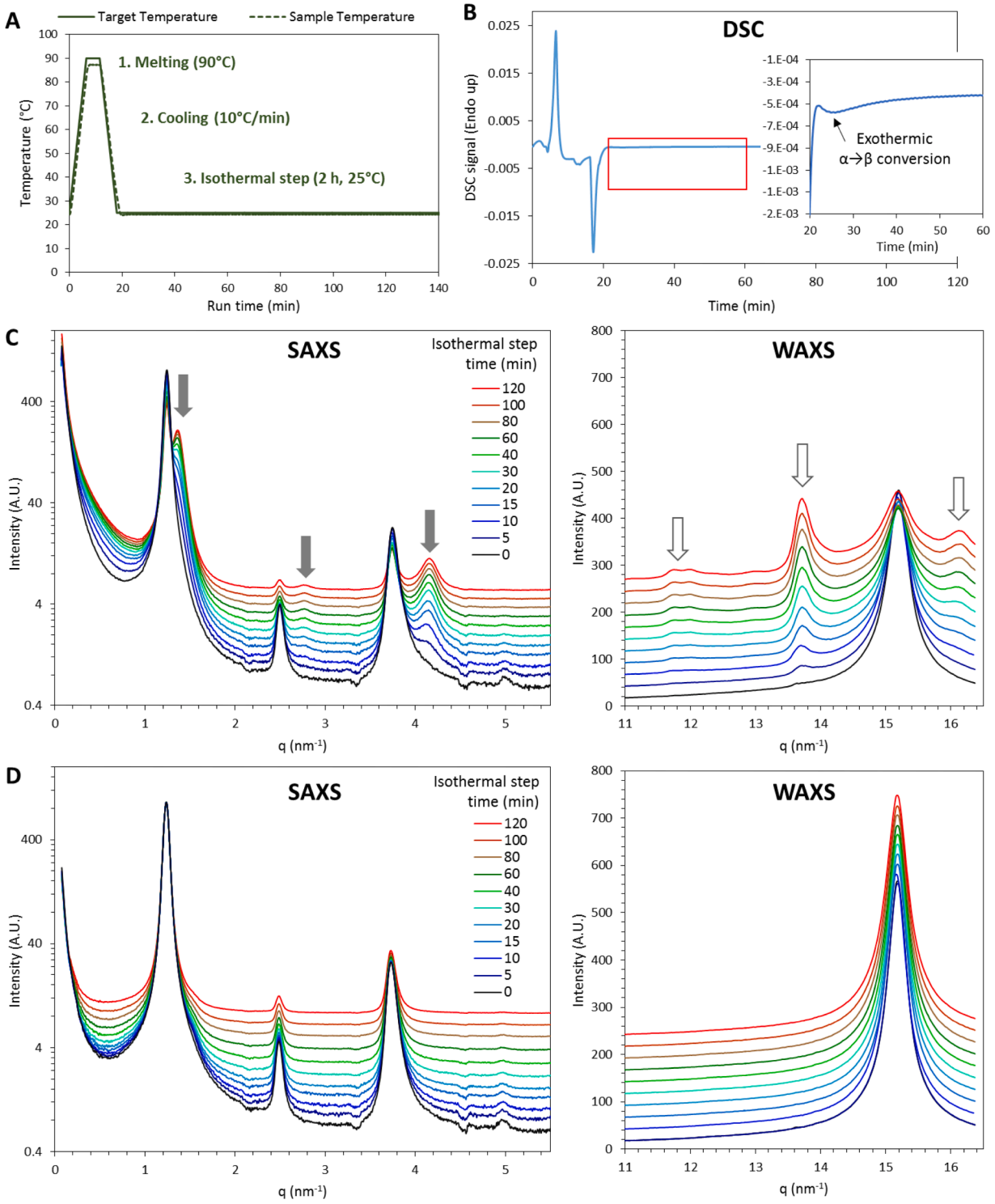

Fig. 3. (A) Thermal profile used for the isothermal crystallization experiment by simultaneous synchrotron SAXS/WAXS and DSC measurements. (B) DSC signal of SSS_IM during isothermal crystallization experiment with zoom in on the first 60 min of the isothermal phase. (C) SAXS and WAXS data of SSS_IM during isothermal crystallization (2 h, 25 °C). (D) SAXS and WAXS data of SSS during isothermal crystallization (2 h, 25 °C).

for crystallite size up to about 100–200 nm (Canchanya-Huaman et al., 2021; Londoño-Restrepo et al., 2019). The calculated crystallite thickness of the reference SSS samples were 87.75 nm and 112.04 nm for α-SSS and β-SSS, respectively.

MPs without additives crystallized in α-SSS with similar nanoplatelets size (in the range 80–93 nm) to the reference α-SSS (Table 2). Conversely, the β-phase developed during storage was characterized by a decreased size as compared to that of the reference β-SSS sample. The crystallite size values of SSS in MPs with additives (Table 2) were lower than pure SSS either in the α- or β-form. Distinct differences were detected comparing the samples containing the various additives, and specifically IM showed the largest crystallite size, EO and OA showed similar intermediate values while MCT was characterized by the smallest size. These differences can be related to the different rate at which the additive promoted the polymorphic conversion and/or to a different molecular mobility of SSS molecules in each SSS/additive

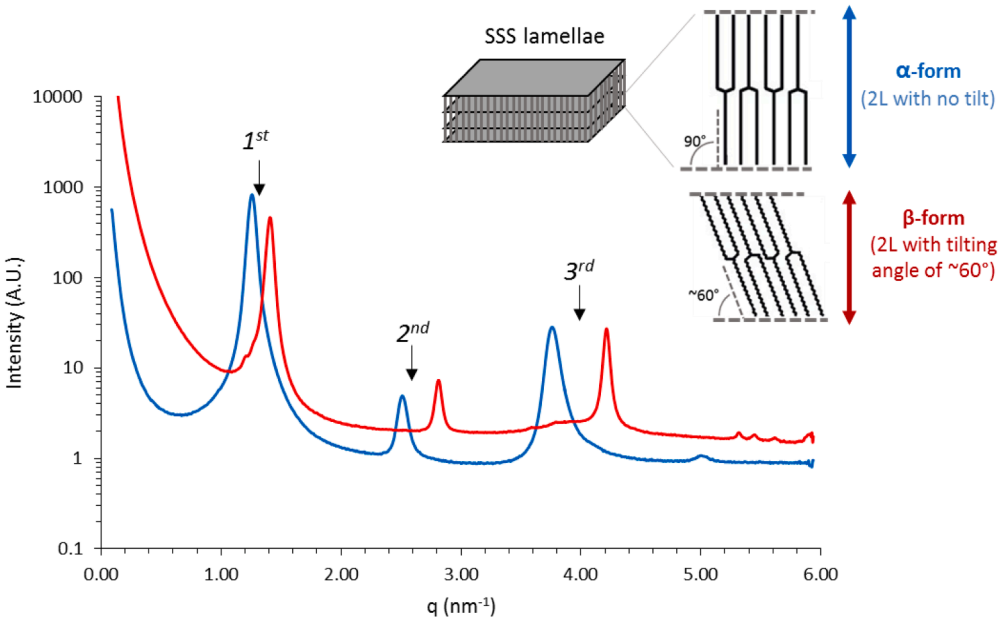

Fig. 4. SAXS pattern of the α-form and the β-form of tristearin and the scheme of their lamellar organization.

Table 1
Composition of the produced MPs batches.

Sample name	Composition (% w/w)					
	SSS	EO	IM	OA	MCT	CAF loading
SSS	100	–	–	–	–	–
SSS_EO	95	5	–	–	–	–
SSS_IM	95	–	5	–	–	–
SSS_OA	95	–	–	5	–	–
SSS_MCT	95	–	–	–	5	–
SSS_CAF15	85	–	–	–	–	15
SSS_EO_CAF15	80.75	4.25	–	–	–	15
SSS_IM_CAF15	80.75	–	4.25	–	–	15
SSS_OA_CAF15	80.75	–	–	4.25	–	15
SSS_MCT_CAF15	80.75	–	–	–	4.25	15
SSS_CAF30	70	–	–	–	–	30
SSS_EO_CAF30	66.5	3.5	–	–	–	30
SSS_IM_CAF30	66.5	–	3.5	–	–	30
SSS_OA_CAF30	66.5	–	–	3.5	–	30
SSS_MCT_CAF30	66.5	–	–	–	3.5	30

Table 2
Values of lamellar thickness and crystallite size of SSS-MPs containing crystal modifiers before (t_0) and after storage (t_6) calculated from SAXS data.

Sample name	Time	Polymorph	Lamellar thickness (Å)	Crystallite size (nm)
SSS	t_0	α	51.0	91.51
	t_6	α	50.6	80.33
		β	46.3	83.32
SSS_EO	t_0	β	44.9	58.47
	t_6	β	44.8	70.31
SSS_IM	t_0	β	44.8	68.53
	t_6	β	44.7	78.68
SSS_OA	t_0	β	44.9	58.64
	t_6	β	44.8	64.06
SSS_MCT	t_0	β	45.1	52.00
	t_6	β	45.0	56.45

system. The influence of each additive on the average number of stacked lamellae at t_0 and at t_6 can be appreciated in Fig. 5. During storage, SSS molecules rearrange in order to decrease the overall energy of the system by increasing the number of stacked lamellae, i.e. crystal growth

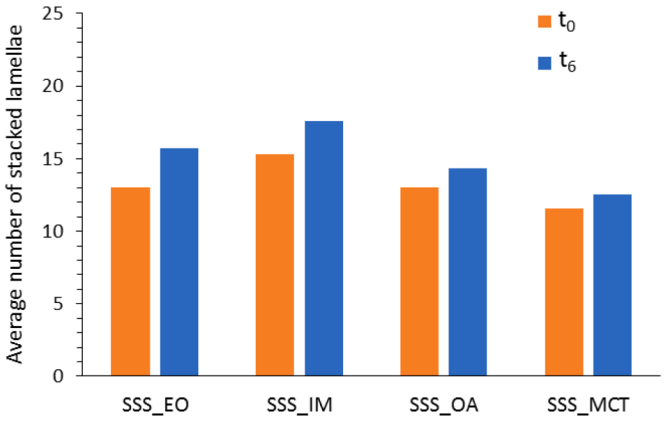

Fig. 5. Average number of stacked lamellae in each crystallite of MPs of SSS with 5 % crystal modifiers (SSS_EO, SSS_IM, SSS_OA, SSS_MCT) at t_0 and after storage (t_6).

(Lopes et al., 2015). It can be observed that the trend in the number of lamellae observed at t_0 for each SSS/additive system (MCT<OA≈EO-<IM) is maintained after storage, although an overall increase in the crystallite size was detected. Crystal growth phenomena have been previously observed for hot melt coated formulations with tripalmitin-polysorbate 65 mixture, with increases of up to 5–7 lamellae after 1 month of storage at accelerated conditions (40 °C/75 % RH) (Schertel et al., 2021a). In the present study, the increase was minor (of about 1 lamella) in samples with OA and MCT, and more pronounced (of about 3 lamellae) for MPs with EO and IM.

3.3. Production and characterization of CAF-loaded MPs

MPs with 15 % or 30 % w/w of CAF, consisting in particles of full solid lipid matrix with embedded CAF crystals, were successfully produced by spray congealing. Yield values ranging 62–65 % were obtained for MPs with 15 % drug amount (Table 3). By increasing CAF content at 30 %, the process yield slightly diminished at values of about 50–58 % (Table 3), probably due to the higher viscosity of lipid mixture containing more CAF powder. Overall, such yield values can be considered

Table 3
Yield, drug content and encapsulation efficiency of the CAF-loaded MPs. Yield and drug content values are expressed as mean ± standard deviation.

Sample name	Yield (%)	Drug content (% w/w)*	Encapsulation efficiency (%)*
SSS_CAF15	63.5 ± 6.4	15.5 ± 0.5	103.6
SSS_EO_CAF15	65.2 ± 4.0	15.3 ± 0.1	101.9
SSS_IM_CAF15	64.1 ± 5.1	15.4 ± 0.2	102.5
SSS_OA_CAF15	65.0 ± 4.5	15.1 ± 0.2	100.5
SSS_MCT_CAF15	62.0 ± 5.0	15.1 ± 0.1	100.7
SSS_CAF30	58.9 ± 8.2	31.2 ± 0.2	104.1
SSS_EO_CAF30	50.1 ± 6.6	29.2 ± 0.9	97.5
SSS_IM_CAF30	53.9 ± 4.4	30.7 ± 1.0	102.5
SSS_OA_CAF30	58.2 ± 1.9	30.1 ± 0.7	100.3
SSS_MCT_CAF30	53.5 ± 9.4	30.4 ± 0.5	101.3

*drug content and relative encapsulation efficiency was determined for MPs with dimensions 250–355 μm.

satisfying considering the small batch size (10 g). CAF-loaded MPs showed optimum drug loading efficiencies, always higher than 97 % (Table 3).

Additional DSC and PXRD of MPs containing CAF confirmed that the presence of embedded drug in the system did not affect the polymorphic conversion caused by the additive. As an example, PXRD of CAF-loaded MPs without (SSS_CAF30) and with crystal modifier (SSS_IM_CAF30) after 48 h from production are reported in Fig. S4.

3.4. Drug release properties of MPs

Solid lipid MPs can prolong the release of the drug by controlling the diffusion of water through the lipid matrix and thus the solubilization of the embedded drug crystals (Kushwah et al., 2020). Release studies were performed on MPs after few days (7 days) from production, defined at time 0 (t_0), when the conversion to the β polymorph was completed; in order to compare the release behavior of samples with same SSS polymorph but with different composition. This would allow to highlight the role of the additives on the release performances.

3.4.1. Drug release in water

Drug release profiles of MPs in water are shown in the first column of Fig. 6. MPs without additives (Fig. 6A) showed a nonlinear release behavior characterized by an initial fast release followed by a much slower rate. Specifically, the burst release observed at the beginning can be related to the CAF crystals loaded on the surface or just below the surface of the MPs, which easily dissolved in water once the MPs are wetted. On this regards, α-SSS is reported to present a higher wettability as compared to the β-SSS (Fang et al., 2007). The release profile from α-SSS MPs is consistent with a recent study where the high wettability and the highly tortuous pore network of α-SSS were related to the initial burst release and to the slow-release phase, respectively (Pluntze et al., 2023). It has been reported, in fact, that the high tortuosity of the pores in α-SSS would be responsible for the more difficult water entrance into the MPs, despite the lower packing density of the α-form compared to the β-form (Pluntze et al., 2023). In order to have information on the mechanism of drug release, the release data were fitted into a range of kinetic models, including zero-order, first-order, Higuchi and Hixson–Crowell models (Table S2). The coefficient of determinations ($R2$) and constants (k) for each model are reported in Table 3. The release profiles of pure SSS MPs fitted the Higuchi kinetic model and this was independent on CAF amount in the formulation. It was previously reported that other BCS class I drugs, such as theophylline (Passerini et al., 2010) or ascorbic acid (Carvalho et al., 2021) embedded in solid lipid MPs followed the Higuchi model, that describes a typical diffusion mechanism-based profile.

In contrast, MPs with additives developed linear profiles without an initial burst release (Fig. 6B–E). In fact, all formulations with additives released about 1–2 % of drug during the first 15 min, as compared to SSS_CAF30 that released more than 13 % of drug during the same time. The addition of crystal modifiers clearly influenced the mechanism of drug release from SSS-MPs. Differently from pure SSS MPs, the release of the formulations with EO, IM and MCT followed the typical zero-order kinetic, where the drug is release at a constant rate. Notably, constant drug release was observed both in case of low ($R^2 = 0.9835$, 0.9952 and 0.9914 for SSS_EO_CAF15, SSS_IM_CAF15 and SSS_MCT_CAF15, respectively) and high ($R^2 = 0.9948$, 0.9971 and 0.9925 for SSS_EO_CAF30, SSS_IM_CAF30 and SSS_MCT_CAF30, respectively) CAF amounts. However, the slope of the straight line obtained by linear regression of the drug concentration–time profiles, corresponding to the rate constant k, varied from 30 to 54 ($*10^{-3}$ min^{-1}) in case of 15 % CAF, to more than 96 ($*10^{-3}$ min^{-1}) for high drug loading. Among the four additives, the release profiles of MPs with OA (Fig. 6D) stood out from the others: both SSS_OA_CAF15 and SSS_OA_CAF30 determined the fastest CAF release in water. Specifically, CAF release rate from MPs containing OA was proportional to the drug concentration, thus following a first-order release kinetics (Table 4). It should be noted that, among the four crystal modifiers, OA is the only one presenting a polar moiety due to the free carboxylic group that makes OA a surface-active molecule (Wellen et al., 2017) with a pKa of approximately 9–10 (Kanicky and Shah, 2002). Both aspects can be responsible for the different release behavior observed for this additive. In fact, changes of the surface properties or of the porosity of the MPs can affect the process of drug diffusion, which is the dominant mechanism of CAF release from solid lipid MPs.

Regarding the influence of drug loading on the release dynamic, the CAF amount in the MPs did not influence the mechanism of drug release, as the same release kinetics were obtained for equivalent formulations having different CAF amounts. Nevertheless, the CAF amount influenced the rate of drug release: as expected, the rate increases with increasing drug loading. In systems with higher drug loading, the porosity created when the drug crystals dissolved facilitated further drug release, thus leading to an increased release profile. Specifically, the impact of CAF amount on the release profiles was much evident in MPs without additives compared to the formulations with additives (e.g., release profiles of SSS_EO_CAF15 and SSS_EO_CAF30 in water were superimposable).

3.4.2. Drug release in biorelevant media

The release performances of MPs in media simulating the gastric and intestinal fasted conditions are showed in the second and third columns of Fig. 6. With the exception of SSS_CAF30, the release of CAF from the MPs increased passing from water to FaSSGF and further increased passing from FaSSGF to FaSSIF. The improvement in drug release passing from simple to biorelevant dissolution media, commonly observed for lipid-based formulations, depends on the effect of enhanced wettability of the lipid surfaces by physiological components of gastrointestinal fluids. This enhancement was more pronounced for MPs containing EO, IM and MCT with respect to those containing OA. Whereas OA determined the highest drug release among the four additives in water, this was not the case in biorelevant media; in these media, the CAF release was similar (in case of SSS_OA_CAF15) or even slower (in case of SSS_OA_CAF30) with respect to the other formulations. Considering the 30 % loaded formulations, for example, the complete release (>98 %) of CAF was achieved in intestinal conditions between 3 and 5 h for MPs containing EO, IM and MCT, whereas a slower release was observed for SSS_OA_CAF30 with only 88 % of drug released in 5 h.

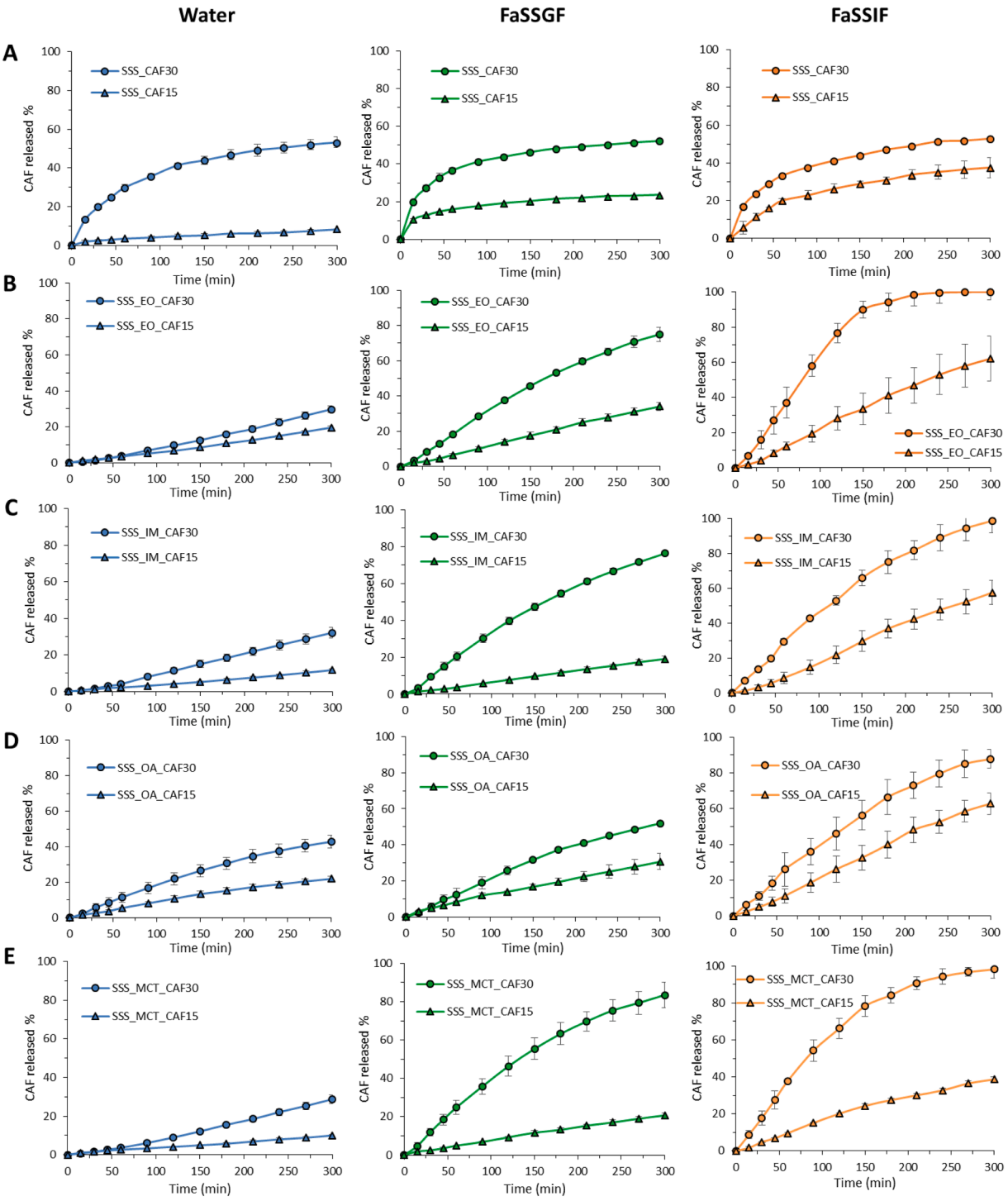

Fig. 6. Drug release profiles of CAF from MPs of SSS alone (A) or with addition of EO (B), IM (C), OA (D) and MCT (E) in water, FaSSGF and FaSSIF after 7 days from production (t_0).

The drug release mechanism in biorelevant media involved two main processes, which are outwards drug diffusion through the lipid matrix and drug release due to erosion of the lipid. Fig. 7 shows the morphology of one MPs sample (SSS_EO_CAF30) before and after release studies. After release in FaSSGF, the surface of MPs containing additives appeared rougher than those before the drug release test, but the structural integrity of the MPs was maintained. This suggests that the difference in drug release with respect to pure water was likely related to the higher wettability of the MPs in FaSSGF due to surface active molecules (e.g. lecithin, bile salts, enzymes) rather than an actual erosion process, which appeared to be limited in FaSSGF. As evident from the SEM analysis, higher erosion and breakage of the particles were observed after the release in FaSSIF. The presence of fragmented and partially degraded MPs was more evident for formulations having EO and IM as crystal modifiers but common to all formulations, suggesting the occurrence of partial emulsification and/or digestion of the lipid by bile salt and pancreatic lipases.

3.4.3. *Stability*

The release studies of MPs with the highest drug loading (30 % CAF)

Table 4
The coefficient of determinations (*R2*) and constants (*K*) obtained by fitting the release data into zero-order, first-order, Higuchi and Hixson–Crowell kinetic models.

Sample	Zero-order		First-order		Higuchi		Hixson	
	R2	K	R2	K	R2	K	R2	K
SSS_CAF15	0.9399	0.023	0.9452	4.34E-05	0.9910	0.451	0.9425	4.00E-04
SSS_EO_CAF15	0.9835	0.054	0.9781	1.10E-04	0.8574	0.970	0.9802	8.81E-04
SSS_IM_CAF15	0.9952	0.038	0.9929	7.51E-05	0.9099	0.692	0.9938	6.06E-04
SSS_OA_CAF15	0.9892	0.075	0.9942	1.59E-04	0.9585	1.413	0.9927	1.26E-03
SSS_MCT_CAF15	0.9914	0.030	0.9910	5.99E-05	0.9483	0.508	0.9913	4.85E-04
SSS_CAF30	0.8420	0.152	0.9074	4.34E-04	0.9765	3.132	0.8873	3.10E-03
SSS_EO_CAF30	0.9940	0.096	0.9887	2.02E-04	0.8805	1.539	0.9908	1.60E-03
SSS_IM_CAF30	0.9971	0.111	0.9918	2.49E-04	0.9029	2.032	0.9942	1.93E-03
SSS_OA_CAF30	0.9927	0.161	0.9991	3.80E-04	0.9514	2.684	0.9978	2.89E-03
SSS_MCT_CAF30	0.9925	0.098	0.9844	2.14E-04	0.8838	1.770	0.9876	1.67E-03

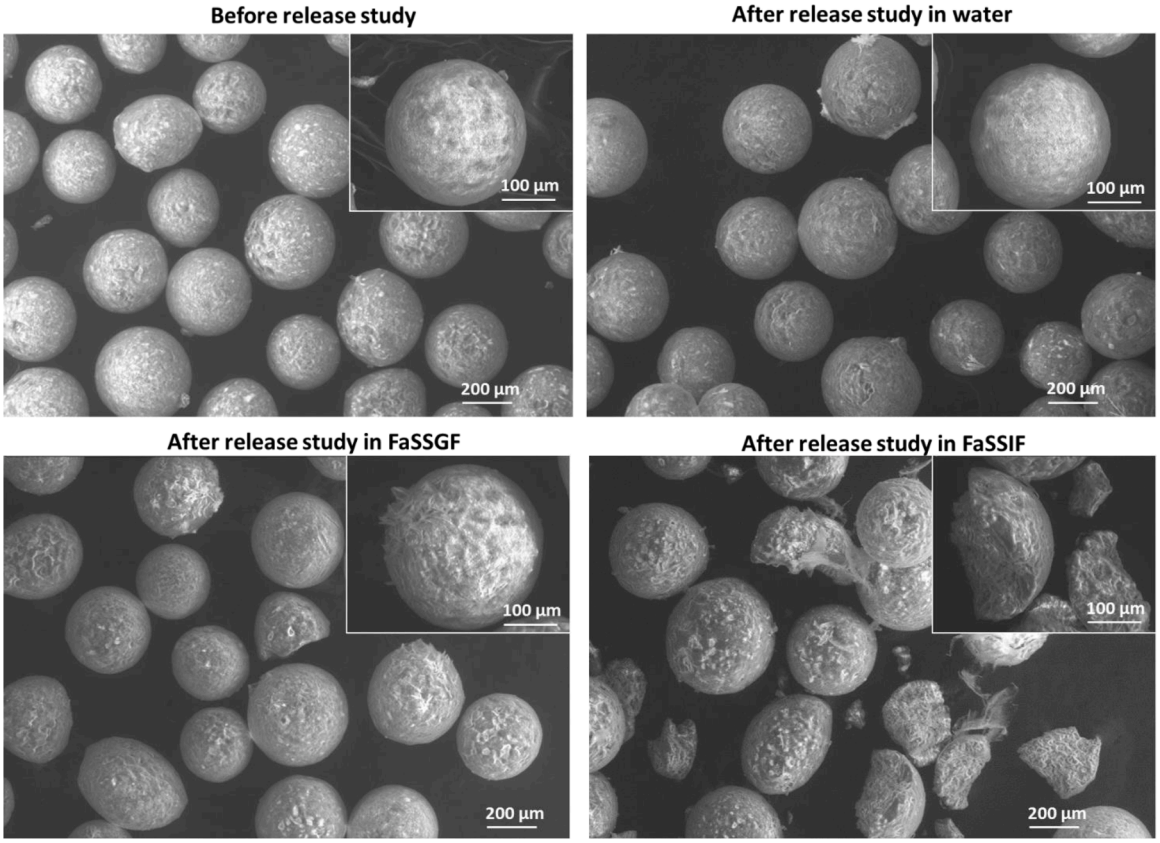

Fig. 7. SEM images of SSS_EO_CAF30 MPs before and after release studies in water, FaSSGF and FaSSIF.

were repeated after 6 months of storage (t_6), using water as dissolution medium. The similarity factors (f_2), comparing the initial release profile with the same after the storage, are listed in Table 5. As evident from Fig. 8A, the drug release from MPs of SSS without additives was dramatically reduced ($f_2 = 27.2$) after storage. This alteration might be the result of the partial α→β conversion of this formulation (Figs. S3 and S4). Accordingly, drug release from β-SSS is lower than that from α-SSS because of two reasons: slow initial wetting due to bloomed surface and limited diffusion of water due to a tight crystalline network with low porosity (Pluntze et al., 2023). On this regard, it should be noted that a considerable reduction in drug release rate was observed despite the modest amount of SSS converted into the β-form after storage. One possible explanation is that the α→β conversion of SSS MPs is more pronounced at the particles surface rather than in the core, so that the limited initial wetting represented the rate-limiting step of drug release

Table 5
Comparison of the release profiles of MPs containing 30 %CAF at t_0 and after 6 months of storage at 25 °C/ 75 % RH (t_6) using the similarity factor *f*2.

Sample	f_2 t_0-t_6
SSS_CAF30	27.2
SSS_EO5_CAF30	49.0
SSS_IM5_CAF30	48.0
SSS_OA5_CAF30	74.2
SSS_MCT5_CAF30	72.4

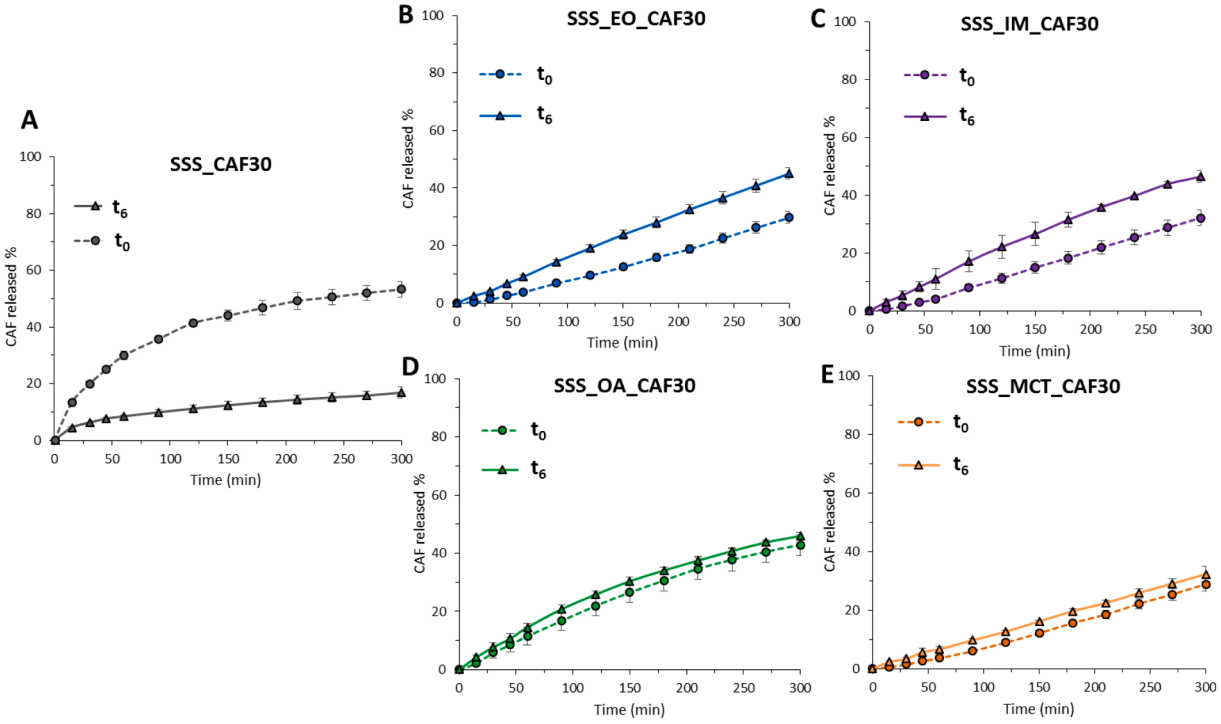

Fig. 8. Comparison of drug release profiles from MPs containing 30 % w/w of CAF consisting of SSS alone (A) or with addition of EO (B), IM (C), OA (D) and MCT (E) before (t_0) and after 6 months of storage (t_6).

process from SSS MPs.

Stability studies of MPs with additives are shown in Fig. 8B–E. Interestingly, a dual behavior is observed: MPs containing IM or EO, the additives that allowed the fastest polymorphic conversion of SSS, depicted an accelerated release after storage with modest but still significant ($f_2 = 49.0$ and 48.0) alterations from those at t_0. Differently, the release performances of MPs containing OA and MCT as crystal modifiers were stable ($f_2 = 74.2$ and 72.4). Since at t_0 MPs with crystal modifiers already exhibited the β-form of SSS, the polymorphic transformation as reason for drug release instability can be excluded. Therefore, modifications in drug release behavior observed after storage for MPs SSS_EO_CAF30 and SSS_IM_CAF30 must be the result of time-dependent alterations of the lipid crystalline structure. Specifically, the crystal growth process observed for MPs containing crystal modifiers can be correlated to the accelerated drug release observed for these samples. In fact, lipid rearrangement into thicker crystallites might result in larger and less tortuous channels/pores that favor water diffusion allowing a more rapid drug release (Kushwah et al., 2020). Accordingly, a correlation was found between the increase in lipid lamellar thickness and drug release alterations, as the two formulations (for MPs with EO and IM) showing the most pronounced (increase of about 3 lamellae) crystal growth also showed unstable release profiles after storage.

4. Conclusions

The polymorphic transformation of SSS-based MPs may be tailored by adding liquid lipids. These additives at concentration of 5 % w/w promoted the transition from the unstable α-form to the stable β-form within 24–48 h from the melting-based production process. This transition, investigated by means of simultaneous synchrotron SAXS/WAXS/DSC analysis, involved a solid-solid phase transformation of SSS without significant variation of the lamellar thickness (d-spacing) of the stable β crystalline arrangement. According to these observations, this strategy is suitable for the production of thermodynamically stable formulations based on solid TAGs. Moreover, the addition of liquid lipids played an important role in the drug release behavior. In water, the presence of crystal modifiers switched the release mechanism from a diffusion-based Higuchi kinetic to a perfect zero-order kinetic. On the other side, the release profiles of MPs increased passing from pure water to the fluids simulating the fasted gastric conditions and the fasted state intestinal environment, where erosion/digestion of MPs was observed. Overall, MPs with additives were able to prolong the drug release over 5 h, which is the ideal behavior for a sustained-release dosage form. After long-time storage, MPs without additives showed a major alteration of drug release due to the slow and uncontrolled α→β transition. Conversely, stable release profiles or minor increases in release rates were observed for MPs with additives after storage. Among the investigated liquid lipids, OA and MCT displayed stable drug release profiles from 30 % CAF loaded-SSS MPs. As MPs were already in the stable polymorphic form (β-SSS), the slightly accelerated drug release can be correlated with time-dependent structural modifications of SSS, that involved a tighter packing of SSS molecules and a crystal growth process, as indicated by lower d-spacings and increased crystallite size, respectively.

It can be concluded that the addition of 5 % liquid lipids to SSS-based MPs resulted a useful formulation strategy to obtain the stable β-form after a reasonable storage time (48 h) from their manufacturing, while maintaining sustained drug release profiles with reduced alteration after storage. Therefore, the results from this study could enable a more rational design and effective green manufacturing of lipid-based pharmaceutical products with tailored and reproducible properties in terms of structure and drug release.

CRediT authorship contribution statement

Serena Bertoni: Conceptualization, Methodology, Investigation, Data curation, Formal analysis, Writing – original draft. **Elena Simone:** Methodology, Data curation, Writing – review & editing. **Stefano Sangiorgi:** Investigation, Writing – review & editing. **Beatrice Albertini:** Methodology, Visualization, Supervision, Data curation, Writing – review & editing. **Nadia Passerini:** Project administration, Funding acquisition, Supervision, Writing – review & editing.

Data availability

Data will be made available on request.

Acknowledgment

We acknowledge CERIC for funding for beamtime on the Austrian SAXS beamline at Elettra Sincrotron Trieste (Italy) under proposals 20217007, 20217066, 20222033 and 20227148 (CERIC). We are grateful to beamline scientists Dr. Barbara Sartori, Dr. Benedetta Marmiroli, and Dr. Sigrid Bernstorff for the help and support with the special setup used for the work.

This project has received funding from the European Research Council (ERC) under the European Union's Horizon 2020 research and innovation programme (grant agreement No 949229, awarded to Dr Elena Simone).

Supplementary materials

Supplementary material associated with this article can be found, in the online version, at doi:10.1016/j.ejps.2023.106650.

References

Abdelbary, G.A., Tadros, M.I., 2008. Design and *in vitro/in vivo* evaluation of novel nicorandil extended release matrix tablets based on hydrophilic interpolymer complexes and a hydrophobic waxy polymer. Eur. J. Pharm. Biopharm. 69, 1019–1028. https://doi.org/10.1016/j.ejpb.2008.01.011.

Acevedo, N.C., Block, J.M., Marangoni, A.G., 2012. Unsaturated emulsifier-mediated modification of the mechanical strength and oil binding capacity of a model edible fat crystallized under shear. Langmuir 28, 16207–16217. https://doi.org/10.1021/la303365d.

Acevedo, N.C., Marangoni, A.G., 2015. Nanostructured fat crystal systems. Annu. Rev. Food Sci. Technol. 6, 71–96. https://doi.org/10.1146/annurev-food-030713-092400.

Albertini, B., Bertoni, S., Perissutti, B., Passerini, N., 2019. An investigation into the release behavior of solid lipid microparticles in different simulated gastrointestinal fluids. Colloids Surf. B Biointerfaces 173, 276–285. https://doi.org/10.1016/j.colsurfb.2018.09.056.

Barthelemy, P., Laforêt, J.P., Farah, N., Joachim, J., 1999. Compritol® 888 ATO: an innovative hot-melt coating agent for prolonged-release drug formulations. Eur. J. Pharm. Biopharm. 47, 87–90. https://doi.org/10.1016/S0939-6411(98)00088-5.

Becker, K., Saurugger, E.-M., Kienberger, D., Lopes, D., Haack, D., Köberle, M., Stehr, M., Lochmann, D., Zimmer, A., Salar-Behzadi, S., 2016. Advanced stable lipid-based formulations for a patient-centric product design. Int. J. Pharm. 497, 136–149. https://doi.org/10.1016/j.ijpharm.2015.11.039.

Bertoni, S., Passerini, N., Albertini, B., 2021. Liquid lipids act as polymorphic modifiers of tristearin-based formulations produced by melting technologies. Pharmaceutics 13. https://doi.org/10.3390/pharmaceutics13071089.

Bertoni, S., Tedesco, D., Bartolini, M., Prata, C., Passerini, N., Albertini, B., 2020. Solid lipid microparticles for oral delivery of catalase: focus on the protein structural integrity and gastric protection. Mol. Pharm. 17, 3609–3621. https://doi.org/10.1021/acs.molpharmaceut.0c00666.

Borde, A.S., Karlsson, E.M., Andersson, K., Björhall, K., Lennernäs, H., Abrahamsson, B., 2012. Assessment of enzymatic prodrug stability in human, dog and simulated intestinal fluids. Eur. J. Pharm. Biopharm. 80, 630–637. https://doi.org/10.1016/j.ejpb.2011.11.011.

Canchanya-Huaman, Y., Mayta-Armas, A.F., Pomalaya-Velasco, J., Bendezú-Roca, Y., Guerra, J.A., Ramos-Guivar, J.A., 2021. Strain and grain size determination of CeO_2 and TiO_2 Nanoparticles: comparing integral breadth methods versus Rietveld, μ-Raman, and TEM. Nanomaterials 11. https://doi.org/10.3390/nano11092311.

Carvalho, JD dos S, Oriani, V.B., de Oliveira, G.M., Hubinger, M.D., 2021. Solid lipid microparticles loaded with ascorbic acid: release kinetic profile during thermal stability. J. Food Process. Preserv. 45, e15557. https://doi.org/10.1111/jfpp.15557.

Fang, W., Mayama, H., Tsujii, K., 2007. Spontaneous formation of fractal structures on triglyceride surfaces with reference to their super water-repellent properties. J. Phys. Chem. B 111, 564–571. https://doi.org/10.1021/jp065589o.

Jaspart, S., Bertholet, P., Piel, G., Dogné, J.-M., Delattre, L., Evrard, B., 2007. Solid lipid microparticles as a sustained release system for pulmonary drug delivery. Eur. J. Pharm. Biopharm. 65, 47–56. https://doi.org/10.1016/j.ejpb.2006.07.006.

Kalnin, D., Lesieur, P., Artzner, F., Keller, G., Ollivon, M., 2005. Systematic investigation of lard polymorphism using combined DSC and time-resolved synchrotron X-ray diffraction. Eur. J. Lipid Sci. Technol. 107, 594–606. https://doi.org/10.1002/ejlt.200501010.

Kanicky, J.R., Shah, D.O., 2002. Effect of degree, type, and position of unsaturation on the pKa of long-chain fatty acids. J. Colloid Interface Sci. 256, 201–207. https://doi.org/10.1006/jcis.2001.8009.

Khan, N., Craig, D.Q.M., 2004. Role of blooming in determining the storage stability of lipid-based dosage forms. J. Pharm. Sci. 93, 2962–2971. https://doi.org/10.1002/jps.20210.

Klein, S., 2010. The use of biorelevant dissolution media to forecast the *in vivo* performance of a drug. AAPS J. 12, 397–406. https://doi.org/10.1208/s12248-010-9203-3.

Kushwah, V., Gomes Lopes, D., Saraf, I., Koutsamanis, I., Werner, B., Zangger, K., Roy, M. C., Bartlett, J.A., Frericks Schmidt, H., Shamblin, S.L., Laggner, P., Paudel, A., 2022. Phase behavior of drug–lipid–surfactant ternary systems toward understanding the annealing-induced change. Mol. Pharm. 19, 532–546. https://doi.org/10.1021/acs.molpharmaceut.1c00651.

Kushwah, V., Lopes, D.G., Koutsamanis, I., Plank, H., Ardelean, I., Sarkar, A., Prpich, A., am Ende, M.T., Schmidt, H.F., Doshi, P., Shamblin, S.L., Laggner, P., Paudel, A., 2020. Evolution of the microstructure and the drug release upon annealing the drug loaded lipid-surfactant microspheres. Eur. J. Pharm. Sci. 147, 105278 https://doi.org/10.1016/j.ejps.2020.105278.

Londoño-Restrepo, S.M., Jeronimo-Cruz, R., Millán-Malo, B.M., Rivera-Muñoz, E.M., Rodriguez-García, M.E., 2019. Effect of the nano crystal size on the X-ray diffraction patterns of biogenic hydroxyapatite from Human, Bovine, and Porcine Bones. Sci. Rep. 9, 5915. https://doi.org/10.1038/s41598-019-42269-9.

Lopes, D.G., Becker, K., Stehr, M., Lochmann, D., Haack, D., Zimmer, A., Salar-Behzadi, S., 2015. Role of lipid blooming and crystallite size in the performance of highly soluble drug-loaded microcapsules. J. Pharm. Sci. 104, 4257–4265. https://doi.org/10.1002/jps.24660.

Lopes, D.G., Koutsamanis, I., Becker, K., Scheibelhofer, O., Laggner, P., Haack, D., Stehr, M., Zimmer, A., Salar-Behzadi, S., 2017. Microphase separation in solid lipid dosage forms as the cause of drug release instability. Int. J. Pharm. 517, 403–412. https://doi.org/10.1016/j.ijpharm.2016.12.040.

Merker, D.R., Daubert, B.F., 1964. The molecular structure in monolayers of saturated triglycerides on water as related to three-dimensional polymorphic forms. J. Am. Chem. Soc. 86, 1009–1012. https://doi.org/10.1021/ja01060a007.

Ollivon, M., Keller, G., Bourgaux, C., Kalnin, D., Villeneuve, P., Lesieur, P., 2006. DSC and high resolution X-ray diffraction coupling. J. Therm. Anal. Calorim. 85, 219–224. https://doi.org/10.1007/s10973-005-7351-y.

Passerini, N., Qi, S., Albertini, B., Grassi, M., Rodriguez, L., Craig, D.Q.M., 2010. Solid lipid microparticles produced by spray congealing: influence of the atomizer on microparticle characteristics and mathematical modeling of the drug release. J. Pharm. Sci. 99, 916–931. https://doi.org/10.1002/jps.21854.

Pluntze, A.M., Cape, J.L., Klaus, N.D., Lyon, D.K., 2023. Control of API release with matrix polymorphism in tristearin microspheres. Int. J. Pharm. 636, 122806 https://doi.org/10.1016/j.ijpharm.2023.122806.

Schertel, S., Salar-Behzadi, S., Karrer, J., Laggner, P., Zimmer, A., 2021a. Impact of polysorbate 65 on tripalmitin crystal growth and release stability of hot melt coated multiparticulate systems. Int. J. Pharm. 607, 120970 https://doi.org/10.1016/j.ijpharm.2021.120970.

Schertel, S., Salar-Behzadi, S., Zimmer, A., 2021b. Impact of surface properties of core material on the stability of hot melt-coated multiparticulate systems. Pharmaceutics 13. https://doi.org/10.3390/pharmaceutics13030366.

Thomsen, L.J., Schæfer, T., Sonnergaard, J.M., Kristensen, H.G., 1993. Prolonged release matrix pellets prepared by melt pelletization I. Process variables. Drug Dev. Ind. Pharm. 19, 1867–1887. https://doi.org/10.3109/03639049309073895.

Van Langevelde, A., Peschar, R., Schenk, H., 2001. Structure of β-trimyristin and β-tristearin from high-resolution X-ray powder diffraction data. Acta Crystallogr. Sect. B 57, 372–377. https://doi.org/10.1107/S0108768100019121.

Vollrath, M., Engert, J., Winter, G., 2017. Long-term release and stability of pharmaceutical proteins delivered from solid lipid implants. Eur. J. Pharm. Biopharm. 117, 244–255. https://doi.org/10.1016/j.ejpb.2017.04.017.

Wellen, B.A., Lach, E.A., Allen, H.C., 2017. Surface pKa of octanoic, nonanoic, and decanoic fatty acids at the air–water interface: applications to atmospheric aerosol chemistry. Phys. Chem. Chem. Phys. 19, 26551–26558. https://doi.org/10.1039/C7CP04527A.